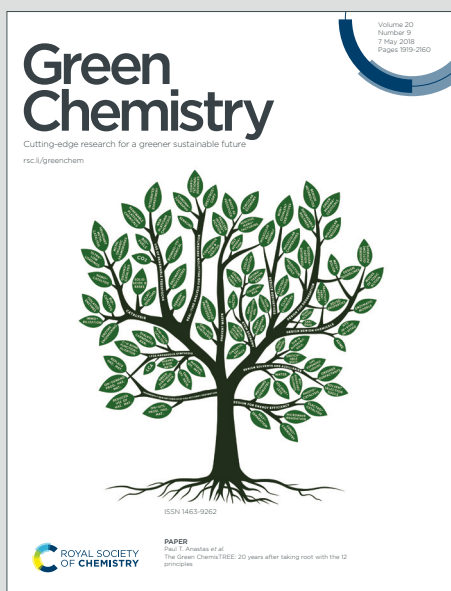


Green Chemistry

Cutting-edge research for a greener sustainable future

Accepted Manuscript

This article can be cited before page numbers have been issued, to do this please use: S. Simeonov, H. Lazarova, M. Marinova and M. Popova, *Green Chem.*, 2019, DOI: 10.1039/C9GC02888A.



This is an Accepted Manuscript, which has been through the Royal Society of Chemistry peer review process and has been accepted for publication.

Accepted Manuscripts are published online shortly after acceptance, before technical editing, formatting and proof reading. Using this free service, authors can make their results available to the community, in citable form, before we publish the edited article. We will replace this Accepted Manuscript with the edited and formatted Advance Article as soon as it is available.

You can find more information about Accepted Manuscripts in the [Information for Authors](#).

Please note that technical editing may introduce minor changes to the text and/or graphics, which may alter content. The journal's standard [Terms & Conditions](#) and the [Ethical guidelines](#) still apply. In no event shall the Royal Society of Chemistry be held responsible for any errors or omissions in this Accepted Manuscript or any consequences arising from the use of any information it contains.

ARTICLE

Achmatowicz rearrangement enables hydrogenolysis-free gas-phase synthesis of pentane-1,2,5-triol from furfuryl alcohol.

Svilen P. Simeonov,^{*a} Hristina I. Lazarova,^a Maya K. Marinova^a and Margarita D. Popova^a

Received 00th January 20xx,

Accepted 00th January 20xx

DOI: 10.1039/x0xx00000x

Abstract: Highly efficient synthesis of pentane-1,2,5 triol, a promising member of the biorenewable C5 alcohols, has been achieved by gas-phase hydrogenation of the derived from furfuryl alcohol Achmatowicz intermediate. The hydrogenations were carried out on monocomponent or bicomponent Ni and/or Pt modified mesoporous silica catalysts. The process features the absence of hydrogenolysis of the furan ring and rendered 100 % selectivity together with additional green chemistry benefits, such as mild and simpler solvent free technology that operates at atmospheric pressure. The bicomponent Ni/Pt modified mesoporous silica catalysts exhibited the highest catalytic activity, with 10Ni1Pt/KIT-6 being the most active, providing up to 100% conversion.

1. INTRODUCTION

Recently, driven by the uncertain availability of fossil resources and the related environmental concerns, substantial steps towards the transition to a bio-based economy have been taken. Due to their large availability from the carbohydrates fraction of the biomass, the furanics quickly emerged as the privilege candidates for technological exploration. Currently, two major platforms, namely 5-hydroxymethyl furfural (HMF)¹ derived from hexoses and furfural² derived from pentoses are considered the most promising. However, despite the intense research, the HMF platform is still in its industrial infancy and is considered a "Sleeping Giant"³ that has to be awakened. In contrast, the furfural platform is currently one of the notable examples of an industrialized biorefinery process.⁴ Apart from furfural, many of its derivatives, for instance, furfuryl alcohol,^{2a} tetrahydrofurfuryl alcohol (THFA),^{2b}, etc. have also reached industrial stage, while others, such as C5 alcohols, are still challenging targets.

The biorenewable C5 alcohols have been recognized as important commodity chemicals for the production of polyesters, polyurethanes, polyethers, and fuel additives.⁵ However, the upgrade of the existing portfolio of furfural derived C5 alcohols usually relies on catalytically challenging hydrolysis or hydrogenolysis of the furan ring.⁶ These transformations usually suffer from harsh conditions and low atom efficiency, which goes against the major principles of green chemistry. In particular, the synthesis of pentane-1,2,5-triol (125PTO) has been rarely achieved from the furfural platform (Figure 1). This observation is intriguing because

125PTO is a homolog of the industrially produced butane-1,2,4-triol thus is a promising target for technological exploration.⁷ 125PTO has been observed as a side product in 19% yield from the hydrogenation of furfural to 1,2-pentanediol in the presence of Rh-Ir alloy.⁸ Later, it has been detected in up to 6.2% conversion and 48.7% selectivity during the hydrogenolysis of THFA over Ni catalysts.⁹ Our group recently reported the synthesis of 125PTO from furfuryl alcohol in outstanding 92% yield.¹⁰ In that work we harnessed the improved reactivity of intermediate **1** (Figure 1), which was conveniently achieved by Achmatowicz rearrangement of furfuryl alcohol and bypassed the problematic C-O bonds hydrolysis or hydrogenolysis. Notwithstanding the high yield of 125PTO and the implementation of flow chemistry methodology, several drawbacks remained namely, the high price of the Pt and Ru catalysts, the very high catalysts/substrate ratios and the large influence of the solvent and the concentration of the feeding solution over the reaction outcome.

With the idea to overcome those drawbacks, we envisaged that the hydrogenation of the Achmatowicz intermediate **1** in gas instead of liquid phase will render higher catalytic activity and simultaneous use of cheap metal catalysts. On the other hand, the solvent-free approach may provide additional green chemistry credits. Given the aforementioned considerations, herein we report the first highly efficient synthesis of 125PTO by gas-phase hydrogenation of **1** over mono or bicomponent transition metal modified mesoporous silica catalysts.

^a Institute of Organic Chemistry with Centre of Phytochemistry
Bulgarian Academy of Sciences
Acad. G. Bontchev str. Bl. 9, 1113 Sofia, Bulgaria
E-mail: svilen@orgchm.bas.bg

† Footnotes relating to the title and/or authors should appear here.

Electronic Supplementary Information (ESI) available: [details of any supplementary information available should be included here]. See DOI: 10.1039/x0xx00000x

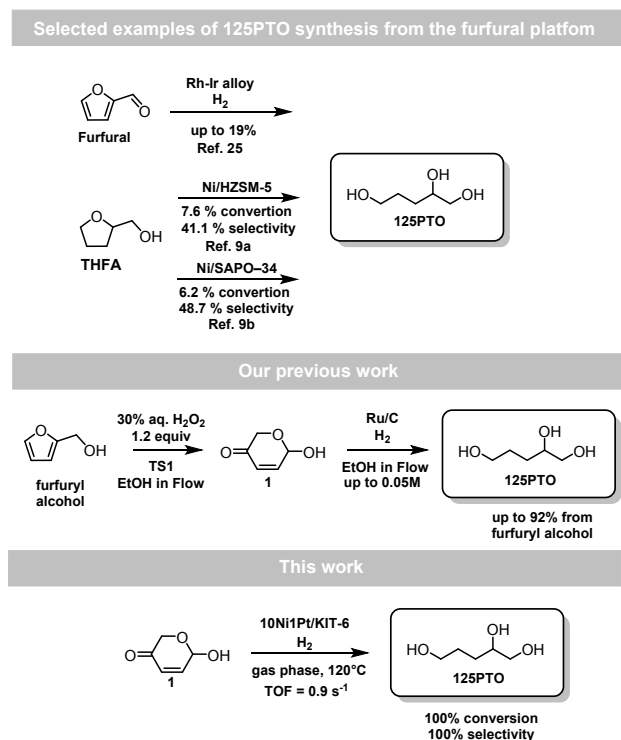


Figure 1. Overview of the 125PTO synthesis from the furfural platform

Supported noble metals and metal oxides have been explored in many catalytic processes.¹¹ Gas-phase hydrogenation reactions have been carried over a large number of mono- and bimetallic catalysts, for instance, Pt, Ni, Pd, Cu, Co and Fe on various supports, such as Al₂O₃, SiO₂, ZrO₂, and active carbon have been explored.¹² Among those supports mesoporous silica materials are of particular interest due to their uniform mesoporous channel structure and high specific surface area. A variety of metal ions (Fe, Ti, V, Cr, Cu, Mn, etc.) has been introduced into silica matrix and the tuneable catalytic properties of the obtained materials have been demonstrated.^{11a, 13} Several parameters such as the preparation method, type of salt precursors and supports strongly influence the state (localization, dispersion, and oxidative state) of the loaded metal species.^{12a, 14} The modification of mesoporous materials by two metals have been used to obtain catalysts owning higher activity and thermal stability as compared to the single oxides. Furthermore, the appropriate ratio between two metals and their amount could facilitate the stabilization of metals as finely dispersed nanoparticles on the silica mesoporous support.^{11d, 15}

Given the enormous utility of the mesoporous silica materials as catalyst support in gas phase hydrogenation reactions for our studies we explored KIT-6 and SBA-15 silicas as supports for Ni and/or Pt nanoparticles formed by incipient wetness impregnation. The catalysts have been fully characterized and their catalytic behaviour is demonstrated.

2. EXPERIMENTAL SECTION

View Article Online
DOI: 10.1039/C9GC02888A

2.1. General

Unless otherwise stated, all reagents were purchased from commercial sources and were used without further purification. The NMR spectra were recorded on Bruker Avance II+ 600 (¹H at 600.13 MHz; ¹³C at 150.92 MHz) spectrometer using CDCl₃ as a solvent.

X-ray patterns were recorded on Philips PW 1810/3710 diffractometer applying monochromatized CuK α radiation (40 kV, 35 mA). Crystallite sizes of the metal oxides were determined by the Sherrer equation evaluating the FWHM values with full profile fitting methods.

Nitrogen physisorption measurements were carried out at 77 K using Quantachrome NOVA Automated Gas Sorption Instrument. Samples were pretreated at 623 K in a vacuum. The pore-size distributions were calculated from the desorption isotherms by the BJH method.

The temperature-programmed reduction-thermogravimetric analysis (TPR-TGA) investigations were performed on Setaram TG92 instrument. The sample (40 mg) was placed in a microbalance crucible and heated in a flow of 50 vol. % H₂ in Ar (100 cm³/min) up to 600°C at 5°C/min and a final hold-up of 1 h. Prior to the TPR experiments the samples were treated in situ in air flow (10°C/min) up to 600°C, followed by a hold-up of 1 h.

Diffuse reflectance spectra in the UV-Vis region were detected at ambient using Jasco V-670 UV-Vis spectrophotometer equipped with NV-470 type integrating sphere using a BaSO₄ disk as reference. The data were collected between 900 and 200 nm wavelengths with 100 nm/min speed, and with 2 nm bandwidth at 1 nm data pitch.

The TEM images were taken on JEOL JEM 2100 TEM (200 kV). The samples were suspended in a small amount of ethanol and a drop of the suspension was deposited onto copper grid covered by carbon supporting film and dried at ambient.

2.1.1. Synthesis of 6-hydroxy-(2H)-pyran-3(6H)-one 1 (Achmatowicz intermediate)

Freshly distilled furfuryl alcohol (20 g) was dissolved in acetonitrile (200 mL) then the catalyst TS-1 (2 g) was slowly added followed by dropwise addition of aq. H₂O₂ (37%, 30 mL). The reaction mixture was heated under stirring at 40°C for 5 h. The progress was monitored by TLC (EtOAc/Hexane = 1:1) until full consumption of the starting material. The crude mixture was filtered, the filtrate was evaporated under vacuum, dissolved in CH₂Cl₂ and dried over MgSO₄ to give **1** in 94% (21.62 g), without further purification. The product was isolated as pale-yellow oil that crystallized in the freezer (-12°C).

2.2. Synthesis of the catalysts

2.2.1. Synthesis of TS-1 catalyst

TS-1 was prepared according to a previously described procedure¹⁶ with modifications. Tetraisopropyl orthotitanate

(0.93 g) and tetraethyl orthosilicate (22.5 g) were dissolved in 50 mL 20 wt% aqueous solution of tetrapropylammonium hydroxide (TPAOH) under vigorous stirring. The resulting mixture was kept at 60°C for 3 h. The final molar ratios in the solution were: $\text{SiO}_2/\text{TiO}_2 = 32.7$, $\text{TPAOH}/\text{SiO}_2 = 0.46$, $\text{H}_2\text{O}/\text{SiO}_2 = 35$. The mixture was transferred into a stainless steel autoclave and heated in an oven at 175°C, under autogenous pressure, in static conditions for 24 h. After cooling to room temperature, the crystalline product was filtered, washed several times with water, dried at 100°C for 2 h, and finally calcined at 550°C in air for 5 h.

2.2.2. Synthesis of SBA-15

Pluronic P123 (12.0 g) was dissolved under vigorous stirring at 35°C in a solution of 37.1 g 37 % HCl in 365.8 g distilled H_2O .¹⁷ After the surfactant was completely dissolved, 24.0 g TEOS was added and the stirring was continued for 24 h. The obtained gel was transferred into an autoclave and kept at 100°C for another 24 h followed by filtration, washing with distilled water and drying at room temperature. For template removal, the obtained powder sample was calcined with a temperature increase of 1°C/min up to 550°C and dwelling times of 2 h at 290°C and 6 h at 550°C.

2.2.3. Synthesis of KIT-6

Pluronic P123 (12.0 g) was dissolved under vigorous stirring at 35°C in a solution of 37.1 g 37 % HCl in 365.8 g distilled H_2O .¹⁷ Then 12.0 g of 1-butanol was added and stirred for an additional 1 h. Then, 24.0 g of TEOS was added and the stirring was continued for 24 h. The formed gel was transferred in a teflon autoclave and heated at 140°C for 24 h. After filtration, washing and drying at room temperature, the obtained powder was calcined in a muffle furnace by heating at a rate of 2°C/min to 550°C for 6 h.

2.3. Preparation of mesoporous silicas transition metal modified analogs.

An incipient wetness impregnation technique with Ni and Pt was applied for loading of 10 wt. % and 1 wt. % metals, respectively. The supports were heated at 160°C for 2 h before the impregnation procedure.

2.3.1. Preparation of monocomponent-modified silicas:

0.275 g $\text{Ni}(\text{NO}_3)_2 \cdot 6\text{H}_2\text{O}$ was dissolved in 2 mL EtOH, added to the silica support (0.5 g KIT-6 or SBA-15) and stirred till dry. Then the sample was dried at 80°C for 18 h.

0.105 g Pt(II) acetyl acetonate was dissolved in 20 mL EtOH and added to the silica support (0.5 g KIT-6 or SBA-15) under stirring at room temperature for 1 h. The solvent was removed under vacuum. Then the sample was dried at 80°C for 18 h. The precursor salts were decomposed in air at 450°C at a rate of 1°C/min for 3 hours. The samples were denoted as 10Ni/SBA-15, 10Ni/KIT-6, 1Pt/SBA-15 and 1Pt/KIT-6.

2.3.2. Preparation of bicomponent-modified silicas:

0.105 g Pt(II) acetyl acetonate was dissolved in 20 mL EtOH and added to the silica support (0.5 g KIT-6 or SBA-15) under stirring at room temperature for 1 h. The solvent was removed under vacuum. Then the sample was dried at 80°C for 18 h to

give 1Pt/KIT-6 or 1Pt/SBA-15, respectively. Then 0.275 g $\text{Ni}(\text{NO}_3)_2 \cdot 6\text{H}_2\text{O}$ was dissolved in 2 mL EtOH, added to 0.5 g 1Pt/KIT-6 or 1Pt/SBA-15 and stirred till dry. Then the samples were dried at 80°C for 18 h. The precursor salts were decomposed in air at 450°C at a rate of 1°C/min for 3 hours. The samples were denoted as 10Ni1Pt/SBA-15 and 10Ni1Pt/KIT-6.

2.4. Catalytic activity measurements

Prior to the catalytic tests, the samples were pretreated for 1 h in H_2 (60 mL/min) up to 400°C. The hydrogenation of 6-hydroxy-(2H)-pyran-3(6H)-one **1** was studied at atmospheric pressure using a fixed-bed flow reactor with H_2 as carrier gas (30 mL/min). 50 mg sample (particle size 0.2-0.8 mm) diluted with 50 mg glass beads of the same diameter, previously checked to be inactive, was tested in each reaction. The reactor itself was a quartz tube of 15 mm inner diameter, with the catalyst bed in the middle. For accurate measurement of the catalyst's temperature a thermocouple was positioned in the catalyst bed. All gas lines of the apparatus were heated continuously at 110°C in order to minimize reactant and products adsorption on the tube walls because of the high boiling temperature of 6-hydroxy-(2H)-pyran-3(6H) **1** (298°C). The H_2 stream was passed through a saturator filled with 6-hydroxy-(2H)-pyran-3(6H)-one **1** and equilibrated at 80°C, ensuring 0.68 g/h reactant content in the H_2 flow. The reactant was fed into the reactor by bubbling through it H_2 flow at 30 mL/min rate. The catalytic tests were carried out in the temperature range of 50-400°C and WHSV=1.1 h⁻¹. The reaction steady state was established after 30 min at each temperature. On-line analysis of the reaction products was performed using HP-GC-FID/TCD with a 30 m HP 5MS capillary column. The catalytic activity of all the studied samples was represented as 6-hydroxy-(2H)-pyran-3(6H)-one conversion (%) and TOF (calculated using the amount of the metallic sites at 120°C).

3. RESULTS AND DISCUSSION

The XRD data of the Ni and Pt modified silica materials in the low two theta region (not shown) confirmed the preservation of the mesoporous structure after the impregnation process. The observed reflections with low intensity in the higher two theta region for the monocomponent Pt supported catalysts indicated the formation of Pt particles with high dispersion whereas reflections with high intensity were registered for Ni-containing catalysts showing the formation of bigger NiO particles. For the bicomponent Ni and Pt supported materials, wide reflections with low intensity, typical for Pt nanoparticles and an intensive peak, typical for NiO (Figure 2), were registered. The formation of smaller NiO particles was evident for the mono- and bicomponent KIT-6 supported catalysts. Peaks with higher intensity were detected for the SBA-15 supported samples thus suggesting the formation of bigger NiO particles.

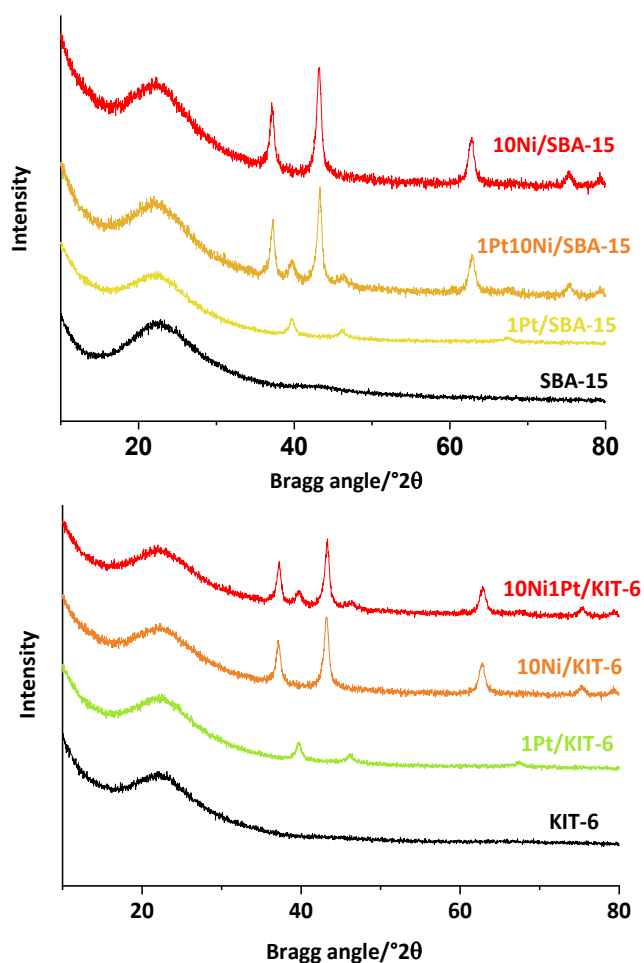


Figure 2. XRD of the KIT-6 and SBA-15 supported samples

The crystallite sizes of the Ni and Pt nanoparticles after ex-situ reduction determined by the Scherrer method are summarized in Table 1. The reduction of the Ni-containing samples led to the formation of metallic nanoparticles with sizes in the interval 10–18 nm whereas smaller Ni nanoparticles (8 nm for 10Ni1Pt/KIT-6 and 15 nm for 10Ni1Pt/SBA-15) were detected on Ni-Pt bicomponent materials. This phenomenon is possibly due to the effects of redispersion of Pt on the Ni nanocrystals on the surface of the silica matrix.

The obtained TEM data was in a good accordance with the XRD observations. The TEM images of 1Pt/KIT-6 (A, C) and 10Ni1Pt/KIT-6 (B, D) (Figure 3) showed that the predominant particle sizes of Pt in 1Pt/KIT-6 are around 6 nm however some clusters of around 12 nm were also observed. The Pt and Ni particles in 10Ni1Pt/KIT-6 were around 5 and 10 nm, respectively.

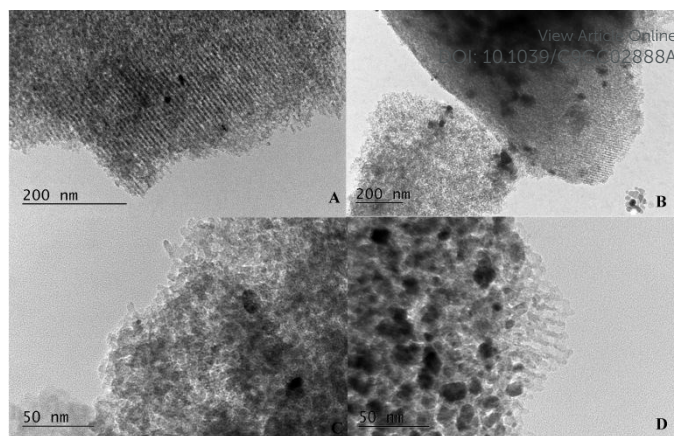


Figure 3. TEM images of 1Pt/KIT-6 (A, C) and 10Ni1Pt/KIT-6 samples (B, D)

The nitrogen physisorption isotherms of the metal-containing silica materials are shown in Figure 4, while the corresponding calculated parameters are summarized in Table 1.

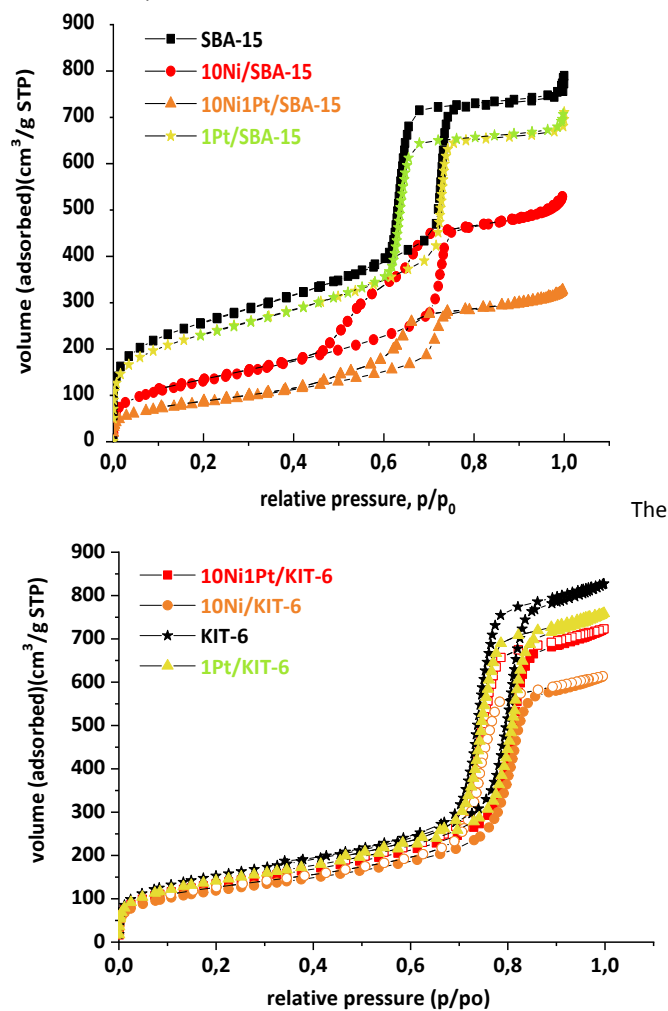


Figure 4. N₂ physisorption of the KIT-6 and SBA-15 supported samples

The isotherms were of type IV (IUPAC classification), with a sharp capillary condensation step at about 0.7 and 0.6 relative pressures, characteristic of KIT-6 and SBA-15 type mesoporous

materials, respectively. On SBA-15 catalysts a parallel, H1 type hysteresis loop was observed.¹⁷⁻¹⁸ This is a characteristic of narrow pore size distribution, indicating the preservation of the mesoporous structure. The impregnation procedure resulted in a decreased BET surface area of the modified KIT-6 and SBA-15 materials (Table 1). Upon impregnation the average pore diameter in KIT-6 samples slightly decreased, whereas in SBA-15 a bimodal pore structure was formed with 6 and 4.7-4.4 nm pore diameters (Table 1). This indicates that some pores were not affected by the impregnation procedure, while other pores are partly blocked by the metal nanocrystals.

Table 1. Physico-chemical properties of the samples

Sample	S_{BET} (m ² /g)	PD ^a (nm)	Pore volume (cm ³ /g)	Size of the metallic particles (nm)	Extent of reduction ^b (%)	TOF at 120°C, s ⁻¹
KIT-6	660	7.9	1.2	-	-	-
1Pt/KIT-6	610	7.9	1.1	4 ^c	100	0.53
10Ni/KIT-6	430	7.8	0.9	10 ^d	80.8	-
10Ni1Pt/KIT-6	490	7.9	1.0	(4 ^c)8 ^d	77.2	0.90
SBA-15	760	6.0	0.9	-	-	-
1Pt/SBA-15	680	6.0	0.9	4 ^c	100	0.46
10Ni/SBA-15	460	4.6	0.7	18 ^d	96.4	-
10Ni1Pt/SBA-15	307	4.8	0.5	(4 ^c)15 ^d	78.8	0.81

^a Pore diameter calculated by BJH method (desorption branch); ^b total weight loss related to the calculated theoretical weight loss for the reduction of the corresponding ion to metallic state; ^c sizes of Pt particles determined by XRD using the Debye-Scherrer method; ^d sizes of Ni particles determined by XRD using the Debye-Scherrer method.

The oxidation and coordination state of the Ni species in the modified KIT-6 and SBA-15 samples were characterized by DR UV-Vis spectra (Figure 5) recorded at room temperature. As was expected no UV-Vis absorbance was evident in the spectra of 1Pt/SBA and 1Pt/KIT-6. The Ni-containing samples present a broad adsorption band, which exhibits a maximum at 245-260 nm with a shoulder at 295 and then a long tail towards longer wavelengths. This zone is typically associated with the O²⁻(2p) → Ni²⁺(3d) charge transfer transition of octahedral Ni²⁺ species, although the first maximum at 260 nm could also be attributed to isolated Ni incorporated in the structure.¹⁹ Several adsorption bands at 430 and 510 nm, and an adsorption zone in the 700-800 nm range, were registered for the 10Ni1Pt/SBA-15. The latter bands are not registered for the 10Ni1Pt/KIT-6 material. These bands in the visible region are associated with several kinds of d-d transitions, superimposed with each other, of Ni²⁺ ions in octahedral local environment in NiO.²⁰ The observed red-shift in the interval 410-580 nm can be ascribed to the well-known quantum size effect, demonstrating the presence of smaller NiO particles in the Ni- and Pt-containing samples as compared to the monocomponent 10Ni/SBA-15 and 10Ni/KIT-6.^{19b} The presence of Pt in the 10Ni1Pt/SBA-15 and 10Ni1Pt/KIT-6 catalysts significantly decreased the broad absorption bands in the regions between 410-580 nm

and 700-760 nm preserving the absorption bands at 260-295 nm which suggests some modification of the NiO species on the catalyst.

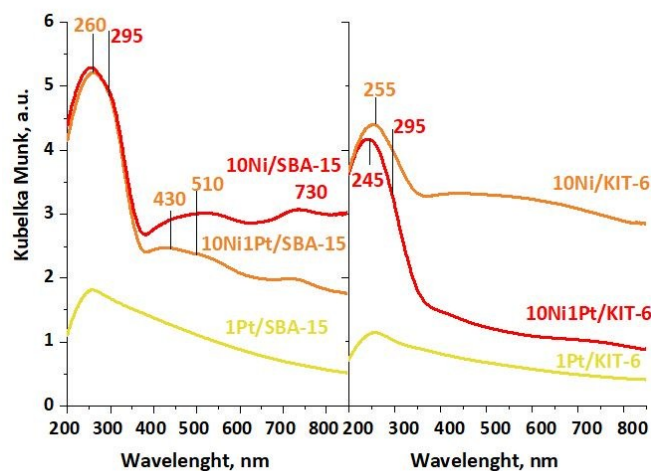


Figure 5. UV Vis spectra of the KIT-6 and SBA-15 supported samples

TPR-TG profiles of the Ni and/or Pt-modified materials are shown in Figure 6. TPR curves of 1Pt/KIT-6 and 1Pt/SBA-15 samples exhibit a low intensive peak at a high reduction temperature. The TPR curve of the 10Ni//KIT-6 sample is characterized by several overlapping peaks between 440 and 534 K and one low intensive peak at 723 K. The first reduction step could be probably related to the reduction of finely dispersed NiO particles. The higher temperature peak could be associated with the reduction of the Ni species incorporated into the wall of the silica matrix during the salt decomposition procedure by reaction with the surface silanol groups.^{12a} The TPR curve of 10Ni/SBA-15 was characterized by two reduction peaks at 565 and 677 K, the latter being more intensive. Bicomponent samples supported on KIT-6 and SBA-15 were reduced in one step at low temperature (the peaks' maximum is at 177°C for 10Ni1Pt/KIT-6 and at 252°C for 10Ni1Pt/SBA-15). The high-temperature peak which was registered for Ni-containing samples disappears in the case of bicomponent ones. Compared to the monocomponent the low-temperature peak for the both bicomponent samples was shifted down by 40-80°C. More prominent shift by 80°C was registered for 10Ni1Pt/SBA-15 with a reduction peak maximum centered at 177°C (Figure 6). The presence of Pt nanoparticles in bicomponent samples facilitated the H₂ dissociation and nucleation thus enabling the reduction of NiO at a lower temperature.²¹

The overall reduction rates of the NiO nanoparticles supported on KIT-6 and SBA-15 (Table 1), were lower than the theoretically required, which can also be explained by the formation of hardly reducible NiO species.

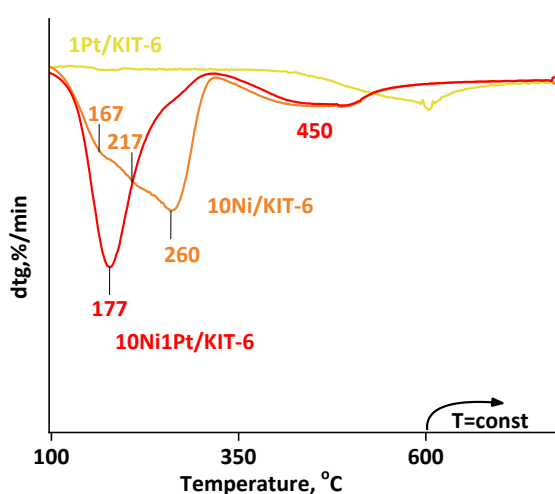
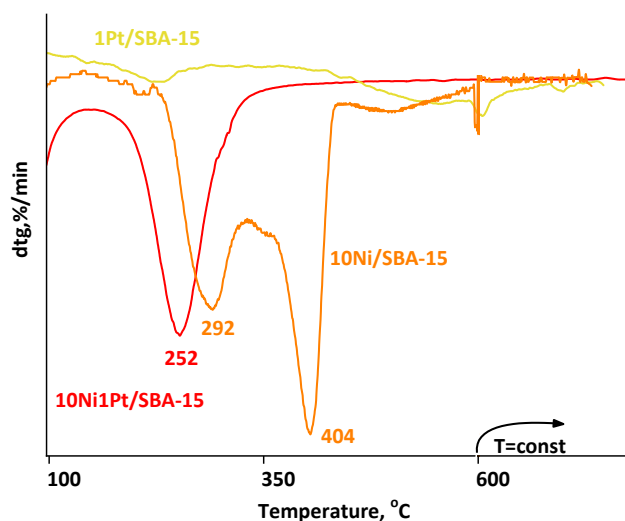


Figure 6. TPR of the KIT-6 and SBA-15 supported samples

With a set of fully characterised catalysts in hand we focused on the gas phase synthesis of 125PTO. To our delight, the use of **1** as an intermediate in this process was beneficial. In contrast with the previous reports (Figure 1) on the synthesis of 125PTO from the furfural platform,⁸⁻⁹ the exclusion of the hydrogenolysis of the parent furan ring and the ease reduction of the olefin and carbonyl moieties in **1** render 100% selectivity in all cases with no evidence of side reactions. In order to validate these results, we studied the stability of **1** by simulating the conditions in the saturator. To this end, we heated **1** under inert atmosphere at 80°C for 20 min. The comparison of the collected ¹H NMR spectra with an authentic sample showed no evidence of decomposition (Figure 7). Furthermore, for the entire set of experiments, we have never observed side peaks by FID neither formation of light gases, such as CO or CO₂, by TCD analysis (all the samples were analysed by GC/FID/TCD). These observations prompt us to believe that indeed the process is highly selective.

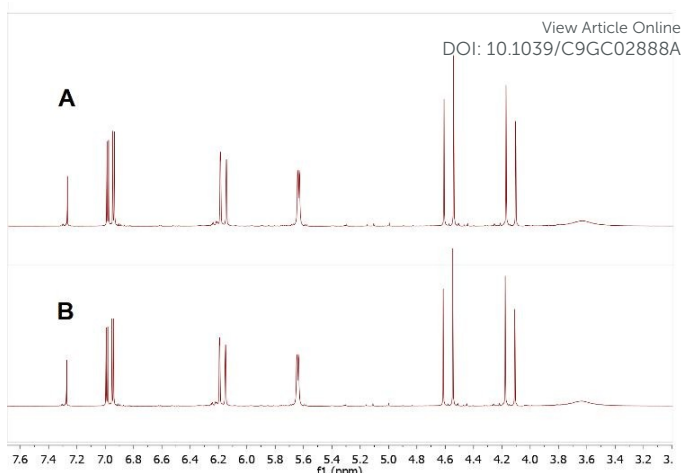


Figure 7. ¹H NMR spectra of **1** A) authentic sample; B) 80°C, 20 min under Argon.

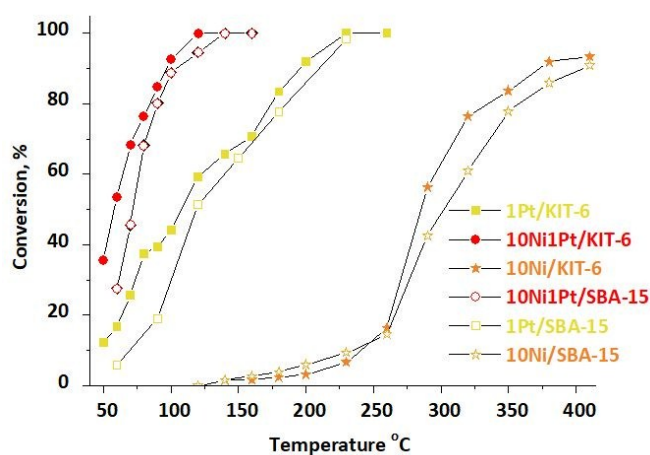


Figure 8. Hydrogenation of **1** to 125PTO vs. reaction temperature

The catalytic activity was dominated by the metal components, while the type of mesoporous silica support exhibited a strong effect on the state and dispersion of the active sites. Monocomponent Pt-modified 1Pt/KIT-6 and 1Pt/SBA-15 catalysts exhibited much higher catalytic activity as compared to monocomponent Ni-modified 10Ni/KIT-6 and 10Ni/SBA-15 (Figure 8). The ability of the metallic Pt to activate hydrogen causing high activity in hydrogenation reactions is well known.²⁰ The simultaneous modification by Ni and Pt resulted in significantly higher activity for 10Ni1Pt/KIT-6 and 10Ni1Pt/SBA-15 which was more pronounced in case of the former (Figure 8). In order to clarify the role of the obtained metallic sites in the catalytic process, the turnover frequency (TOF) data at 120°C was calculated for the catalysts which were active at this temperature (Table 1). 10Ni1Pt/KIT-6 catalyst rendered the highest TOF value thus demonstrating the beneficial synergistic effect of the simultaneous modification with Pt and Ni particles and the pore structure of the KIT-6 material. Moreover, a drop in the activity was registered for the monocomponent Pt-modified 1Pt/KIT-6 and 1Pt/SBA-15 catalysts with time on stream (3 h) whereas the bicomponent

samples exhibited stable activity. This could be explained by preservation of metallic nanoparticles' dispersion (both Pt and Ni) which was validated by the lack of changes in the particle sizes (XRD) of the spent catalysts. Additionally, we performed catalytic tests on 20Ni/KIT-6 and 20Ni1Pt/KIT-6 samples containing bigger Pt (8 nm) and Ni (43 nm for mono component and 35 nm for bicomponent) nanoparticles (XRD). The catalytic data (Figure 9) showed a decrease of the catalytic activity in comparison to their 10%Ni-containing mono- and bicomponent KIT-6 analogues that feature smaller nanoparticles. Moreover, the significantly lower catalytic acidity was registered on 10Ni1Pt/SiO₂ prepared with nonporous SiO₂ carrier (Figure 9) indicating the significant role of the particles' dispersion.

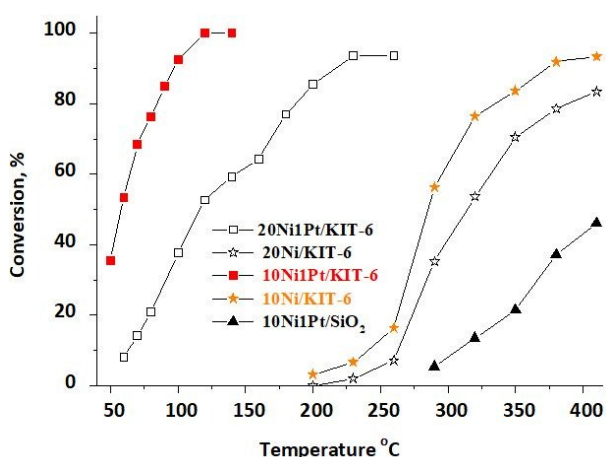


Figure 9. Hydrogenation of **1** to 125PTO on 10Ni/SiO₂, 20Ni/KIT-6 and 20Ni1Pt/KIT-6 vs 10Ni/KIT-6 and 10Ni1Pt/KIT-6

4. CONCLUSIONS

In conclusion, we demonstrated high-yield synthesis of pentane-1,2,5-triol by gas-phase hydrogenation of the derived from furfuryl alcohol Achmatowicz intermediate. A range of newly prepared mono or bicomponent mesoporous SBA-15 and KIT-6 catalysts modified with Pt and/or Ni were fully characterised and explored in a hydrogenolysis-free process that rendered up to 100% conversion and selectivity. Furthermore, we demonstrated that the variation of the pore structure of the supports influences the nature and the dispersion of the formed metal nanoparticles as well as their catalytic activity. The successful penetration of the metal precursors into the bimodal pore structure of KIT-6 led to the formation of more finely dispersed metal nanoparticles than in the open pore structure of SBA-15. The bicomponent catalysts exhibited higher catalytic activity, showing the beneficial effect of the presence of a second metal. Furthermore, our studies provided additional green chemistry benefits, such as mild and simpler solvent free technology that operates at atmospheric pressure. Therefore, we believe that this highly efficient and greener process further highlights the potential of

Achmatowicz rearrangement as a platform transformation for biorefinery.

DOI: 10.1039/C9GC02888A

Conflicts of interest

"There are no conflicts to declare"

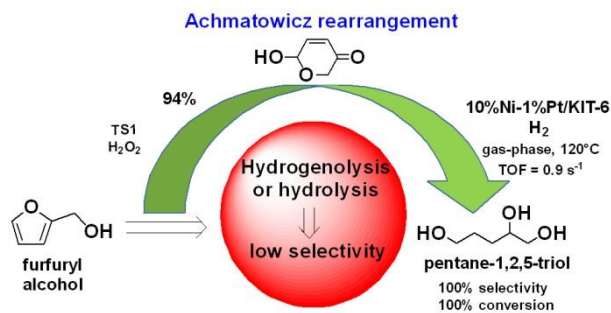
Acknowledgements

The authors would like to acknowledge the financial support from National Science Fund of Bulgaria (grant КП-06-ОП-01/2) and partial support by the Bulgarian Ministry of Education and Science under the National Research Programme E+: Low Carbon Energy for the Transport and Households, grant agreement D01-214/2018. H. Lazarova acknowledges the partial support by the Bulgarian Ministry of Education and Science under the National Research Programme "Young scientists and postdoctoral students" approved by DCM # 577/17.08.2018.

References

- (a) R.-J. van Putten, J. C. van der Waal, E. de Jong, C. B. Rasrendra, H. J. Heeres and J. G. de Vries, *Chem. Rev.*, 2013, **113**, 1499-1597; (b) A. A. Rosatella, S. P. Simeonov, R. F. M. Frade and C. A. M. Afonso, *Green Chem.*, 2011, **13**, 754-793.
- (a) X. Li, P. Jia and T. Wang, *ACS Catal.*, 2016, **6**, 7621-7640; (b) R. Mariscal, P. Maireles-Torres, M. Ojeda, I. Sádaba and M. López Granados, *Energy Environ. Sci.*, 2016, **9**, 1144-1189.
- K. I. Galkin and V. P. Ananikov, *ChemSusChem*, 2019, **12**, 2976-2982.
- C. M. Cai, T. Zhang, R. Kumar and C. E. Wyman, *J. Chem. Technol. Biotechnol.*, 2014, **89**, 2-10.
- D. Sun, S. Sato, W. Ueda, A. Primo, H. Garcia and A. Corma, *Green Chem.*, 2016, **18**, 2579-2597.
- (a) S. Chen, R. Wojcieszak, F. Dumeignil, E. Marceau and S. Royer, *Chem. Rev.*, 2018, **118**, 11023-11117; (b) Y. Nakagawa, M. Tamura and K. Tomishige, *ACS Catal.*, 2013, **3**, 2655-2668; (c) Y. Nakagawa, M. Tamura and K. Tomishige, *Catal. Surv. Asia.*, 2015, **19**, 249-256.
- (a) Y. Cao, W. Niu, J. Guo, M. Xian and H. Liu, *Sci. Rep.*, 2015, **5**, 18149; (b) G. Wang, B. Guo and R. Li, *J. Appl. Polym. Sci.*, 2012, **124**, 1271-1280.
- S. Liu, Y. Amada, M. Tamura, Y. Nakagawa and K. Tomishige, *Catal. Sci. Technol.*, 2014, **4**, 2535-2549.
- (a) E. Soghrati, C. Choong, C. K. Poh, S. Kawi and A. Borgna, *ChemCatChem*, 2017, **9**, 1402-1408; (b) E. Soghrati, T. K. C. Ong, C. K. Poh, S. Kawi and A. Borgna, *Appl. Catal. B Environ.*, 2018, **235**, 130-142.
- S. P. Simeonov, M. A. Ravutsov and M. D. Mihovilovic, *ChemSusChem*, 2019, **12**, 2748-2754.
- (a) S. Singh, R. Kumar, H. D. Setiabudi, S. Nanda and D.-V. N. Vo, *Appl. Catal.*, 2018, **559**, 57-74; (b) B. Fotoohi, M. Kazemzad and L. Mercier, *Ceram. Int.*, 2018, **44**, 20199-20210; (c) M. Popova, Á. Szegedi, Z. Cherkezova-Zheleva, A. Dimitrova and I. Mitov, *Appl. Catal.*, 2010, **381**, 26-35; (d) Á. Szegedi and M. Popova, *J. Porous Mat.*, 2010, **17**, 663-668; (e) S. Song,

- S. Yao, J. Cao, L. Di, G. Wu, N. Guan and L. Li, *Appl. Catal. B Environ.*, 2017, **217**, 115-124.
- 12 (a) Á. Szegedi, M. Popova, V. Mavrodinova, M. Urbán, I. Kiricsi and C. Minchev, *Micropor. Mesopor. Mat.*, 2007, **99**, 149-158; (b) D. Sun, A. Ohkubo, K. Asami, T. Katori, Y. Yamada and S. Sato, *Molecular Catalysis*, 2017, **437**, 105-113; (c) V. V. Kumar, G. Naresh, M. Sudhakar, C. Anjaneyulu, S. K. Bhargava, J. Tardio, V. K. Reddy, A. H. Padmasri and A. Venugopal, *RSC Adv.*, 2016, **6**, 9872-9879; (d) L. Liu, H. Lou and M. Chen, *Appl. Catal., A*, 2018, **550**, 1-10; (e) K. Tie, X. Pan, T. Yu, P. Li, L. He and X. Bao, *J. Energy Chem.*, 2019, **31**, 154-158.
- 13 (a) A. Taguchi and F. Schüth, *Micropor. Mesopor. Mat.*, 2005, **77**, 1-45; (b) J. Liang, Z. Liang, R. Zou and Y. Zhao, *Adv. Mater.*, 2017, **29**, 1701139; (c) P. Sudarsanam, E. Peeters, E. V. Makshina, V. I. Parvulescu and B. F. Sels, *Chem. Soc. Rev.*, 2019, **48**, 2366-2421.
- 14 (a) V.-C. Niculescu, G. Paun and V. Parvulescu, *Materials Today: Proceedings*, 2019, **7**, 443-448; (b) J. Grams, N. Potrzebowska, J. Goscianska, B. Michalkiewicz and A. M. Ruppert, *Int. J. Hydrog. Energy*, 2016, **41**, 8656-8667; (c) S. Chen, C. Ciotonea, A. Ungureanu, E. Dumitriu, C. Catrinescu, R. Wojcieszak, F. Dumeignil and S. Royer, *Catal. Today*, 2019, **334**, 48-58.
- 15 P. C. Rath, M. Mishra, D. Saikia, J. K. Chang, T.-P. Perng and H.-M. Kao, *Int. J. Hydrog. Energy*, 2019, **44**, 19255-19266.
- 16 M. G. Clerici, G. Bellussi and U. Romano, *J. Catal.*, 1991, **129**, 159-167.
- 17 D. Zhao, J. Feng, Q. Huo, N. Melosh, G. H. Fredrickson, B. F. Chmelka and G. D. Stucky, *Science*, 1998, **279**, 548.
- 18 M. Grün, K. K. Unger, A. Matsumoto and K. Tsutsumi, *Micropor. Mesopor. Mat.*, 1999, **27**, 207-216.
- 19 (a) P. Dai, T.-t. Yan, X.-x. Yu, Z.-m. Bai and M.-z. Wu, *Nanoscale Res. Lett.*, 2016, **11**, 226; (b) Y. Volokitin, J. Sinzig, L. J. de Jongh, G. Schmid, M. N. Vargaftik and I. I. Moiseevi, *Nature*, 1996, **384**, 621-623.
- 20 S. A. Karakoulia, E. Heracleous and A. A. Lappas, *Catal. Today*, 2019, DOI: 10.1016/j.cattod.2019.04.072
- 21 C. M. N. Yoshioka, T. Garetto and D. Cardoso, *Catal. Today*, 2005, **107-108**, 693-698.



Hydrogenolysis-free gas-phase hydrogenation of an Achmatowicz intermediate provided pentane-1,2,5-triol in 94% overall yield from furfuryl alcohol